Disposable pH Sensor on Paper Using Screen-Printed Graphene-Carbon Ink Modified Zinc Oxide Nanoparticles

Akshaya Kumar Aliyana, Priyanka Ganguly, Ajay Beniwal, Naveen Kumar S K and Ravinder Dahiya, *Fellow IEEE*

***Abstract*— Estimation of pH is vital to assess the biochemical and biological processes in a wide variety of applications ranging from water to soil, health, and environment monitoring. This work reports a screen-printed flexible and disposable pH sensor using the impedimetric method. The pH sensor was fabricated by screen printing Graphene-Carbon modified Zinc Oxide based active layer on a paper substrate and shows nearly three orders of change in impedance magnitude in the pH range of 2 – 9. The sensor was carefully designed using COMSOL® Multiphysics software to understand the influence of electrode geometry and the electrical potential developed across the structure. The developed sensor was used for pH monitoring of soil and exhibited high sensitivity of 5.27 kΩ /pH (2-8) with a correlation coefficient (R^2) of 0.99. Finally, an IoT-enabled smart pH detection system was implemented for continuous pH monitoring for potential application in digital agriculture. The outcome demonstrates that the presented flexible and disposable pH sensor could open new opportunities for monitoring of water, product process, human health, and chemical (or bio) reactions even using small volumes of samples.**

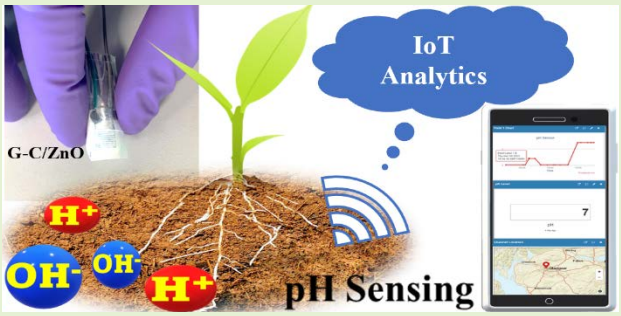

***Index Terms*— pH sensor; Disposable Sensor; Graphene; Screen Printing; IoT Analytics**

I. Introduction

The pH value is a vital parameter that is needed to assess the biochemical and biological processes in a wide variety of applications ranging from water to soil, health, and environmental monitoring[1][2]. Monitoring of pH assures drinking water safety, the survivability of marine organisms, homeostasis maintenance and wastewater remediation[3]. Likewise, pH sensing has received considerable interest in recent years as part of wearable systems for the early prediction of diseases through the non-invasive analysis of bodily fluids like sweat, saliva, and urine[4][5]. This work has particularly reported on the continuous soil condition monitoring application. Maintenance of an appropriate level of pH in soil could help to enhance crop yields as well as the fight against biotic and abiotic stresses. Thus, monitoring soil pH plays a critical role in the enhancement of crop productivity and huge demand exists for disposable pH sensors in smart agriculture[6].

A wide range of pH sensing techniques ranging from optical to electrochemical to physicochemical methods has been developed using materials such as metal oxides, polymer, and carbon-based composites. However, not all are suitable for in situ soil condition monitoring in agricultural applications, where disposable sensors capable of providing single and/or multiple reliable measurements over a short duration are preferred[7]. As an example, traditional glass-based pH sensors are bulky, and it is difficult to have them in a portable and biocompatible form to enable a large number of sensor deployments in smart agriculture settings[8]. The widely reported metal oxides (e.g., RuO_2) for pH sensing applications are toxic and non-biocompatible[9][10][11]. Deployment of such sensors in large numbers could also aggravate the challenges related to electronic waste.

This work is supported in part by the British Council and Department of Science and Technology (DST) through the Newton-Bhabha Mobility scheme, Engineering and Physical Science Research Council (EPSRC) through Engineering Fellowship (EP/R029644/1), and European Commission through grant references (H2020-MSCA-ITN-2018-813680). For the purpose of open access, the authors have applied a Creative Commons Attribution (CC BY) license to any Author Accepted Manuscript version arising.

A.K Aliyana and S.K Naveen Kumar are with the Department of Electronics, Mangalore University, Mangalore, 574199, India.
P. Ganguly, A. Beniwal, and R. Dahiya are with Bendable Electronics and Sensing Technologies (BEST) Group, University of Glasgow, G12 8QQ, UK. (Corresponding author: Ravinder Dahiya; e-mail: ravinder.dahiya@glasgow.ac.uk).

In this context, ZnO offers a better alternative as it is non-toxic, biocompatible, easy to synthesize, and abundantly available [12][13]. It is one of the amphoteric materials and therefore can create oriented dipoles or surface bonds by adsorbing (H^+ and OH^-) ions in pH solution [14]. However, the high temperature (>120 ^{0}C) needed for the synthesis of ZnO nanostructures does not go well with disposable substrates such as paper and textiles. As a result, ZnO-based sensors are often reported on rigid and non-degradable substrates, which makes it difficult to use them in practical applications [15][16]. The pH sensors developed from such materials on disposable, flexible, biocompatible substrates can be used for a broad range of biosensing applications [17][18][19][20]. The paper-based pH sensor presented here addresses this need.

The disposable pH sensor reported here is realized on a paper substrate. The sensor consists of the interdigitated electrode (IDE) realized by screen-printing a graphene-carbon (G-C) ink on a paper substrate. The biocompatible ink serves as a perfect substitute for the toxic metallic inks used for printing without compromising the conductivity of the printed electrodes to a broader extent. The printed structure is further modified by the addition of a ZnO layer, which can exhibit polar and nonpolar active surfaces. Further, their high crystallinity nature makes them attractive for pH sensors active layer [15]. The ZnO modified screen printed electrodes on a paper substrate for pH sensing are not reported yet. The sensor design (electrode geometry) was finalized with COMSOL® Multiphysics simulation studies, which were carried out to understand the influence of electrical potential developed across the IDE structure. The use of an optimized IDE pattern enabled a faster response (10 sec) and high sensitivity (5.27 kΩ /pH) of the presented sensor. The performance of sensors with modified electrodes was evaluated over a range of pH 2 to 9 and the disposability of the device was also studied. The sensor displayed almost complete depletion within 45 days. Finally, the potential applicability of the presented sensor for digital agriculture was evaluated by measuring the pH of various soil samples, the real-time transfer of wireless data using an IoT system and displaying the data on a smartphone using the web application.

II. Materials and Methods

A. Materials

The interdigitated electrodes (IDE) are developed using graphene-carbon ink (C2171023D1: Graphene Carbon Ink:BG04, Sun Chemical). Commercially available Zinc Oxide (ZnO) nanoparticles dissolved in ethanol (C2H5OH, MW: 46.07 g/mol, Thermo Scientific) solvent are used for fabricating the active layer for pH sensing.

B. Screen printing

The interdigitated electrodes were developed on a paper substrate using screen printing (Screen Stencil Printer C920 from AUREL Automation). The IDEs printed on the paper had three configurations i.e., single layered, double layered and triple layered. The optimized active layer configuration was obtained by analyzing their pH sensing output. The 2 wt. % solution of ZnO nanoparticles in ethanol solvent was prepared by 2 hours of ultrasonication at room temperature. The 0.5 mL of this solution was drop casted on all three (single, double, and triple layered) IDE structures. The process was repeated 10 times to attain the desired thickness. The ZnO nanoparticles modified G-C IDE was calcinated at 60˚C for 24 hours. Further,

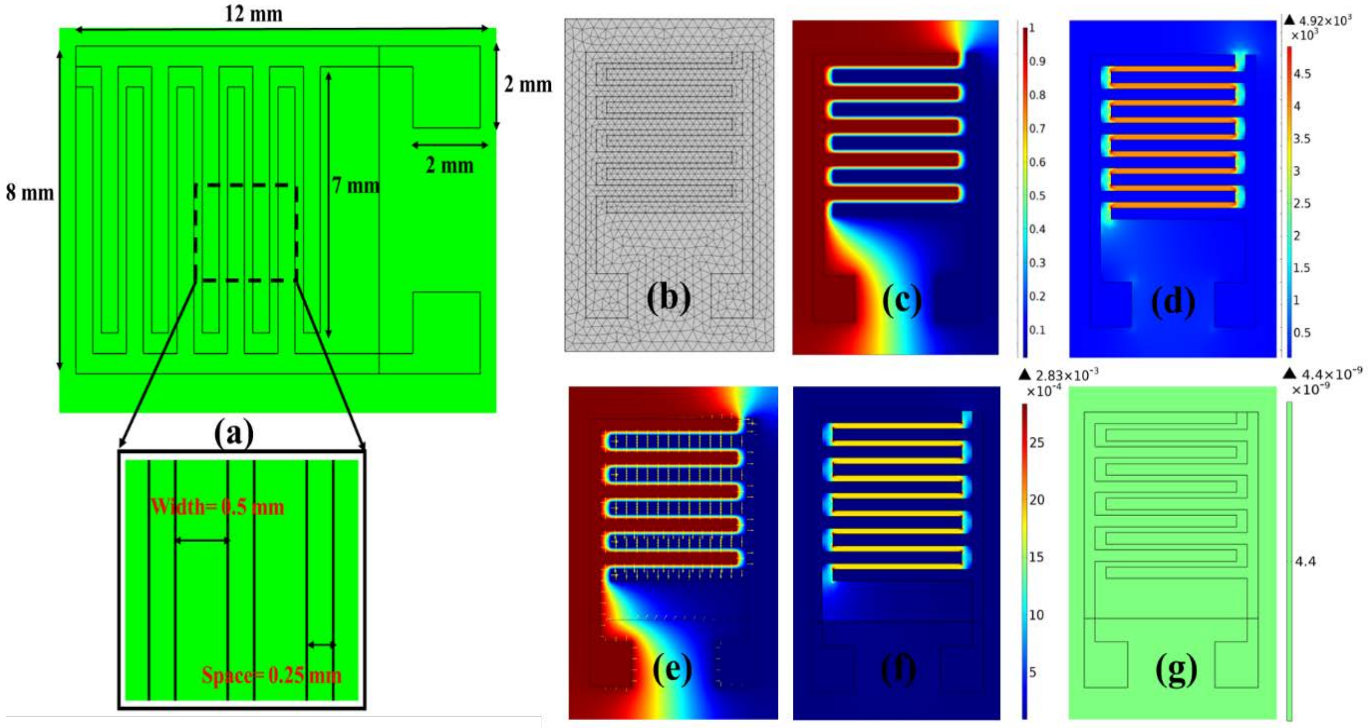

Fig. 1. (a) Schematic design of the interdigitated electrode (IDE) platform for pH sensing, (b) Finer physics-controlled mesh of the device for COMSOL simulation, (c) Electric field displacement of the device for the applied electric potential of 1 V, (d) Two-dimensional average electric field potential plot of the device, (e) Direction of electric field (logarithmic arrow lines) in the device (f) Two-dimensional average current density plot of the device and (g) Two-dimensional total electric energy plot of the device.

the connection points are obtained using wiring followed by dielectric placement to insulate the connection. Later the sensor is utilised for the pH monitoring process.

C. Characterization

The morphological and structural characteristics of the spin coated ZnO layer is analysed using scanning electron microscopy (FEI Nova) and X-ray diffraction (XRD P'Analytical X'Pert with Cu Kα ($\lambda = 1.541$ Å)). The screen-printed IDE structure is imaged using an optical microscope (Nikon, Eclipse LV100ND). The hydrophilicity of the ZnO layer is analysed using contact angle measurement. Further, the electrical characteristic i.e., change in impedance response is monitored using the LCR meter (Keysight E4980AL, Precision LCR Meter).

D. pH sensing set-up

The pH sensing performance of the developed sensor is monitored using the Keysight E4980AL. The pH samples are prepared corresponding to the target range i.e., pH 2 to pH 9. Electrochemical impedance spectroscopy is carried over the range of 40 Hz to 100 kHz using a 1 Vpp sine wave for the target pH range. The list sweep parameters such as impedance magnitude (R-X) and double layer capacitance (C_{dl}) are extracted in the single trigger computation. All the measurements are carried out at room temperature (25 ± 2 ˚C). To analyses the performance of the developed sensor towards soil pH monitoring, the soil samples with a pH value of 2, 4, 6 and 8 were used. Initially, the impedance of the sensor is monitored under normal ambient conditions followed by monitoring the change in impedance magnitude towards prepared soil samples (pH 2-8). The schematic illustration of the pH sensing set-up is shown in Fig. 7(b).

III. Result and Discussion

A. COMSOL simulation

The strength of the electric field and potential of the sensor electrodes were studied by using AC/DC module under the COMSOL® Multiphysics software. The total area of the sensor is kept constant (12 mm x 8 mm) to incorporate the 10 individual electrodes with 0.5 mm width and 0.25 mm interspace for the electrodes (Fig. 1a). Graphene-Carbon was used as the active material and air acted as the bottom layer of the electrode. Modeling was supported using finer physics-controlled mesh (Fig. 1b). To compute the electric field displacement of IDEs, the electric potential (Bias Voltage =1 V and Frequency =1000 Hz) was sequentially applied to the working electrodes (WE) and reference electrodes (RE). The two-dimensional electric potential plot of devices is shown in Fig. 1c. Electric potential is supreme at the digits of the WE and varies from 4.92 kV to 0 V (Red to Blue) moving from WE to the RE. Color gradients in middle confirm the electrostatic potential variation as it moves from the middle of the field. The device with the 10 interdigitated electrodes design pattern generated the maximum average electric field potential of 4.92 kV (Fig. 1d). Fig. 1e shows the direction of the electric field (logarithmic arrow lines) to confirm the charge particle displacement in the device. The maximum current density of 2.83 x 10^{-3} A/m^2 (Fig. 1f) and total electric energy of 4.4 x 10^{-9} J (Fig. 1g) are detected at the WE, which influences the output response of the fabricated device[21].

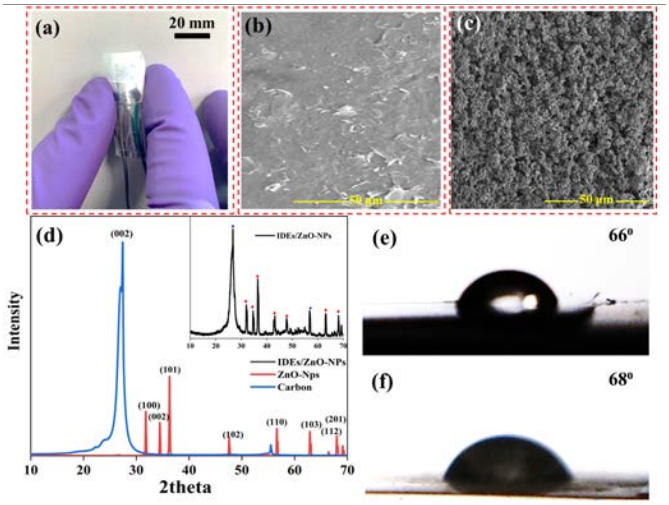

Fig. 2. (a) Screen-printed G-C electrode modified ZnO-NPs active layer-based pH sensor. SEM images of the (b) G-C electrode and (c) G-C electrode modified ZnO-NPs active layer at 50 μm magnifications; (d) XRD spectrum for G-C electrode modified ZnO-NPs active layer and contact angle measurement of the (e) G-C electrode and (f) G-C electrode modified ZnO-NPs.

B. Material characterization

The screen-printed G-C modified ZnO-NPs sensing layer-based pH sensor is shown in Fig. 2a. The surface morphology of the G-C based IDE and ZnO-NPs based active layer is investigated using scanning electron microscopy (SEM) images as shown in Fig. 2 (b-c). The G-C ink printed surface (Fig. 2b) across the electrode is shown and it displays the random distribution of carbon and graphene network. On the other hand, the images taken at lower magnification for ZnO modified printed electrode shows distributed spherical particles (Fig. 2c). While the image at higher magnification helps in estimating the average particle size to be around 200 nm (Fig. S1). The diffractograms of the printed electrode, ZnO nanoparticles and the modified printed electrode with ZnO are displayed in Fig. 2d. The printed electrode diffractogram (blue line) displays a peak of carbon around 27^0. However, the broadness in the peak observed is contributed by the presence of graphene nanosheets. While the diffractogram of ZnO (red line) displays the traditional peaks at 31.7^0, 34.4^0, 36.1^0, 47.4^0, 56.4^0, 66.3^0, 68.1^0 and 69.2^0 corresponding to (100), (002), (101), (102), (110), (103), (112) and (201) respectively. The results agree with the standard peaks observed for hexagonal wurtzite structure (ICDD card no: 36-1451). The sharp peaks indicate the high crystallinity of the nanoparticles. The peaks observed for the modified printed electrode with ZnO (black line in the inset) show the presence of a combination of both peaks (Carbon and ZnO).

The contact angle measurement using the sessile drop technique of the bare IDE and by modifying the surface of the IDE is shown in Fig. 2 (e-f). The angle calculated for the bare IDE and the modified IDE is measured to be 66^0 and 68^0 respectively. The G-C ink exhibits a hydrophilic nature and no change in the surface was observed on modifying with ZnO.

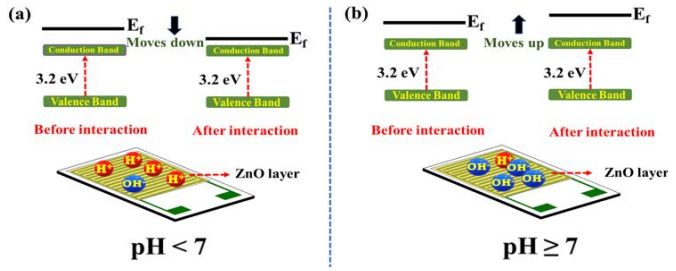

Fig. 3. Schematic illustration of pH sensing mechanism of different pH levels (a) pH < 7 and (b) pH ≥ 7.

The optical image was taken for sensor 1 at a 5X magnification aided in measuring the width (~500 mm) and the interspace gaping (~250 mm) between the electrodes as shown in Fig. S2.

C. Evaluation of pH sensing performance

The pH of any solution is determined by the presence of H^+ and OH^- ions. The material used for the sensing layer defines the overall response observed. In the present work, ZnO is utilised as the sensing material and deposited above the printed IDE structure. Table S1 provides a comparative analysis of the present work with the state of the art. The impedimetric response of the sensor increases with the increase in the pH values. With the increase in the impedance value, the decrease in capacitance value is predicted [22]. However, on closer inspection of the data collected, there is no evident relation observed between the change in pH and capacitance. Thus, emphasizing the contribution of the conductance of the ZnO comes into play, rather than the overall capacitance [23]. This suggests that with the increase in the OH^- ions the overall conductance of the system reduces. The change in the impedimetric response of the sensor could be proposed as the change in the density of states (DOS) of ZnO with the introduction of the hydroxyl ions [24]. The DOS could essentially observe a trough and subsequently lead to an increase in the band gap (Eg), by increasing the distance between the fermi level (E_f) (Fig. 3) [25]. ZnO being an n-type semiconductor has excess electrons contributed by Zn atoms[14]. Being one of the amphoteric materials and therefore being able to create oriented dipoles and surface bonds by adsorbing (H^+ and OH^-) ions form the pH solution [26].

Based on the COMSOL studies, it is found that the IDE structure with ten interdigitated electrodes with 0.5 mm width and 0.25 mm interspace for the electrodes displayed maximum electric potential response. The same design is further used to screen print three different types of IDE altering the number of layers and further modified with ZnO NPs. Sensor 1 i.e., single G-C layer, sensor 2 i.e., double G-C layer, and sensor 3 i.e., triple G-C layer analyzed by varying pH 2 to pH 9.

The blank sensor impedance spectra shows an inversely proportional response with frequency since the impedance of a capacitor is inversely proportional to the frequency [27][28]. The |Z_max| values, estimated as 2.19×10^6 Ω, 1.62×10^6 Ω and 1.60×10^6 Ω, served as the starting point for the parameterization of sensors 1, 2 and 3 respectively. The response curve (Fig. S3) displays the predominant effect of thickness on the impedance characteristics of the G-C electrode modified with the ZnO active layer. The overall impedance is reduced with increasing thickness of the G-C electrode;

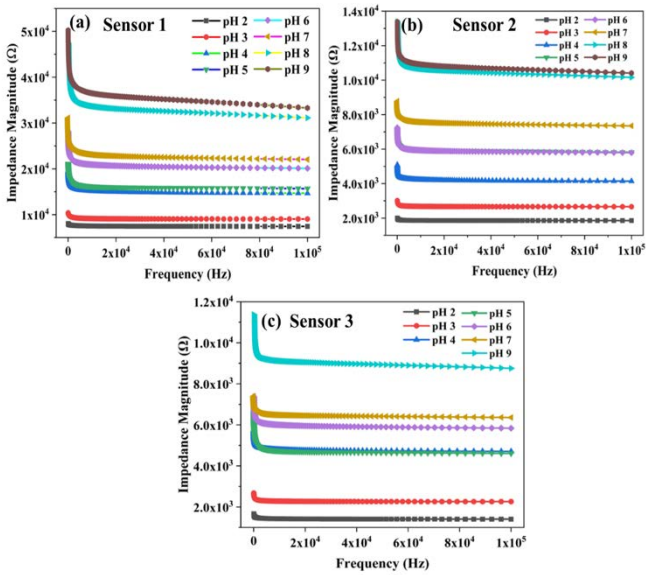

Fig. 4. Comparative analysis of pH sensing performance of (a) sensor 1; (b) sensor 2 and (c) sensor 3 from pH 2-9.

however, the stability and the overall response are compromised too. Fig. 4 shows the impedimetric performance of the sensor (1, 2 and 3) across continuous frequency sweep (40 Hz – 100 kHz) in pH adjusted solutions, prepared at physiological conditions from HCl and KOH buffer (25 ± 2 ˚C, 4.4 mol %). A proportional decrease in impedance magnitude was observed with respect to the increase in the frequency level (40 Hz – 10 kHz). Furthermore, with the increase in frequency up to 100 kHz, the impedance value drastically decreases and holds up. A similar pattern was observed for all three sensor conditions (Fig. 3. a, b, and c). Even though |Z_max | is higher at a lower frequency (40 Hz) level, the target signals are quite unstable and stabilizes only as the frequency level is increased from 40 Hz to 1 kHz, which records the |Z_max | value of ~50.2 KΩ. Optimal parameters such as the |Z_max | and the frequency dependency of |Z| are found to vary from device to device. |Z_max | values for sensor 1 is ~ 36.8% higher compared to sensor 2 and its ~ 38.83 % higher for sensor 3. |Z_max | values were comparatively stable for sensor 1 with a maximum variation of ± 2 KΩ. On the other hand, the function of pH (i.e., dissociation of H^+ and OH^- ions) clearly reflected the change in ions concentration in the dielectric medium and causes a change in the sensor impedance magnitude allied with the protonation (<pH 6) and deprotonation (>pH 8) of the buffer. The rate of change in impedance magnitude is highest at neutral (pH 7) to alkaline (pH 9) transition conditions, whereas it is very gradual in acidic medium (pH 2-6). In addition to that, the sensitivity of the sensors (1, 2 and 3) is estimated from the characteristics curve of average impedance magnitude vs pH (Fig. S4). Moreover, the sensors are also plotted for some of the selected stable frequency conditions (1 kHz, 5 kHz, 10 kHz, and 50 kHz) as shown in Fig. S5, Fig. S6, and Fig. S7. It can be observed that the electrochemical response of the device shows a linear increase of impedance magnitude with an increase in the pH levels. The correlation coefficient (R^2) and sensitivity of the fabricated device are calculated in the selective range and recorded in Table 1.

Upon close inspection of the responses, the sensor 1 results

displayed appreciable sensitivity (6.21-3.99 KΩ/pH), which is about four folds higher than that of sensors 2 and 3. Moreover, the sensitivity and the correlation coefficient (R^2) estimated at 1 kHz are stable and also the highest among all the other tabulated values. A sequential decrease in the sensitivity value is observed as the frequency level increases. Accordingly, sensor 1 with an applied frequency condition of 1 kHz is judged as the most sensitive and stable device for pH sensing in the desired pH range (pH 2-9) and investigated further for characterization and soil application studies.

TABLE I
CHANGE IN SENSITIVITY AND CORRELATION COEFFICIENT (R^2) COMPARISON BASED ON PH SENSOR TYPE AND FREQUENCY

Sensor Type	Sensitivity (kΩ/pH)	Adj. R square	Frequency (kHz)
Sensor1	6.21	0.94685	1
	4.68	0.9461	5
	4.21	0.94808	10
	3.99	0.95153	50
Sensor 2	1.69	0.94457	1
	1.4	0.9545	5
	1.34	0.95806	10
	1.30	0.95984	50
Sensor 3	1.30	0.92961	1
	1.10	0.95305	5
	1.05	0.95487	10
	1.01	0.95365	50

Further, the relative response of the pH sensor 1 is determined at each intermediate pH level. The relative response vs pH graph is shown in Fig. 5 for the selected frequency level. The relative response value is observed at the lowest of 1 for pH 2, which gradually increases up to 5 for pH 9. The change in relative response for the selected frequency condition (1, 5,10 and 50 kHz) does not show any more significant alterations even at the higher pH range. Therefore, the sensor response could be found ideal for the pH range 2-9. The repeatability and the reproducibility of the fabricated sensor are studied. Fig. 6a displays the multiple trials performed on the same sensor at various pH levels. The impedance magnitude (Ω) of the sensor has been measured three times (Trial 1, Trial 2, and Trial 3) and the results confirm that the impedance response of the sensor is affected slightly for the multiple trials.

However, the response starts to deteriorate after 5 trials, as the sensing layer deposited on the surface of the printed IDE starts to wear off. Hence, the sensors could be limited to up to 3 cyclic usages. This also shows the disposability nature of the fabricated sensor. While the reproducibility study performed for three different sensors modified with ZnO has been studied under similar conditions (Fig. 6b). The impedance magnitude (Ω) vs pH concentration response of the three different sensors (sensors I, II and III) are shown in Fig. 6b. The error margin between the different sensors is estimated to be 2.67 % and 2.23%, respectively for sensor II and III devices, when compared with sensor I. The error margin is in an acceptable range as it is <3% for long range pH detection. These results display a good stable response observed and thus the fabricated sensor could be utilised for continuous and repetitive detection. The rate of adsorption is dependent on the availability of free holes or electrons on the surface of nanostructures. In the case of lower pH values, the H^+ ions form a partial surface bond with the excess electron available in the structure [25][26]. This

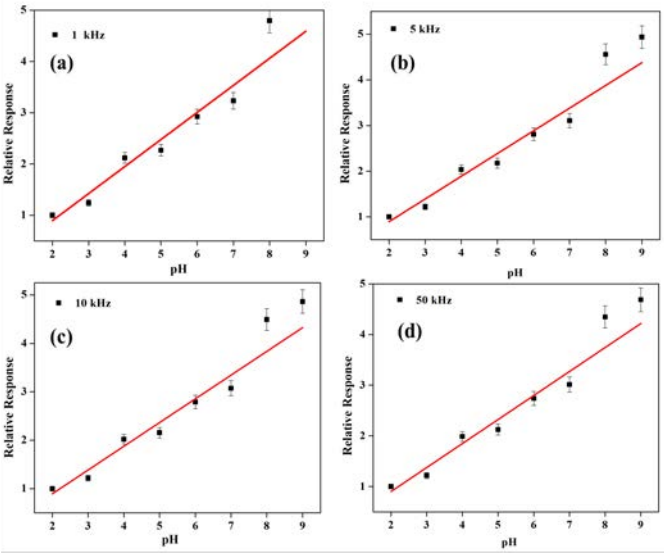

Fig. 5. Relative pH response of sensor 1 for the selected frequency (1, 5, 10 and 50 kHz).

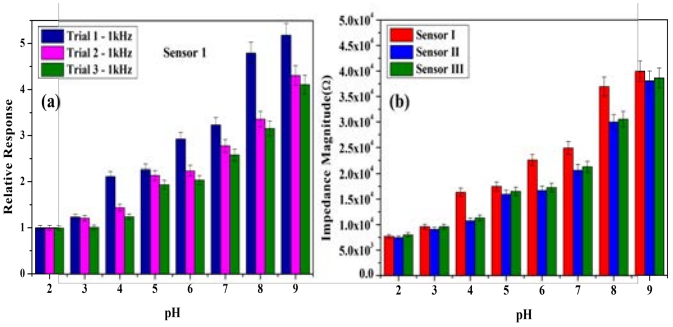

Fig. 6. (a) Repeatability study of the sensor 1 for multiple trials (1-3) and (b) reproducibility performance of multiple sensors (I, II and III) at a frequency of 1 kHz

results in lower impedance (or higher conductance) and faster response. At neutral and basic pH values, the presence of OH^- ions are equal or higher respectively. These negative ions lead to higher impedance (or lower conductance) and delayed response [25]. The delayed response has been previously reported for basic/neutral pH solutions in the case of a few metal oxides [24]. This is also observed in the real time monitoring of the pH.

D. Sensor application

The developed sensor is further tested for monitoring the soil pH level as shown in Fig. 7b. The monitoring of the soil conditions (pH, electrical conductivity (EC), Organic Carbon (O.C) and Macronutrients (NPK)) will provide key information to improve resource utilization and to maximize farming outputs[22]. Here, pH is one of the important parameters to be assessed. The soil samples for pH estimation are obtained from the University Glasgow, Scotland, the UK, and the test samples are prepared using standard protocol for the pH measurement. Fig. 7a shows the four different soil samples with pH values of 2 to 8. Initially, the sensor is placed under normal ambient conditions and the impedance of the sensor is monitored. Further, the sensor is deployed on the surface of the prepared soil samples (pH 2-8) and the change in impedance magnitude is monitored as shown in Fig. 8a.

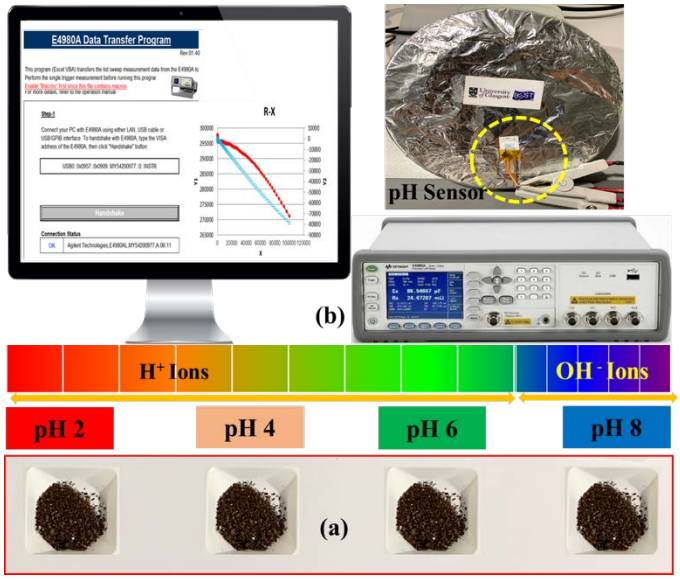

Fig. 7. The application of pH sensor for soil pH analysis (a) Prepared soil samples with different pH levels (2-8) and (b) Set up for monitoring the soil pH level

The sensing characteristics of the sensor toward soil pH levels are validated by comparing the calibrated pH level with obtained soil pH level, which is estimated from the data collected. The change in impedance magnitude is calculated and confirms that the sensing performance of the device shows a linear increase in impedance magnitude (7.9 - 48 kΩ) with the increase of pH (2-8) value. To calculate the linear fit and sensitivity of the sensor, a corresponding curve of average impedance magnitude vs soil pH level characteristics is plotted and is displayed as in Fig. 8a. The fabricated pH sensor yielded a sensitivity of 5.27 kΩ /pH in the pH range of 2 to 8 with a correlation coefficient (R^2) estimated to be 0.99. As seen in the plot (Fig. 8b), a linear pH response is observed for pH 2-8. The obtained relative response value is well matched with the primary calibration results performed on the pH buffered solutions and the sensor output remains stable even at a higher pH range. Therefore, the sensor response could be found ideal for real time soil pH monitoring applications. Furthermore, a soil burial degradation test is performed for studying the disposability of the fabricated sensor. The sensor is kept inside the compost soil for a prolonged duration and disintegration of the sensor is observed across 45 days. The degradation of the sensor throughout the 45 days is displayed in Fig. 9. The sensor is observed at regular intervals, as it is thoroughly washed using distilled water and imaged for reporting the disintegration/degradability of the sensor.

D. Real-time sensing and monitoring of pH level

Real time pH level monitoring system is facilitated using the Node MCU microcontroller platform. As shown in Fig. 10, the wireless system consists of a fabricated pH sensor, signal processing unit, inbuilt Wi-Fi module for data transmission and power supply unit. The system was powered by a 3 V supply and a 32-bit microcontroller integrated with an ESP-12 module (Wi-Fi SoC). System design parameters include the repeatability and stability of the change in impedance measurements of the calibrated pH sensor to predict the

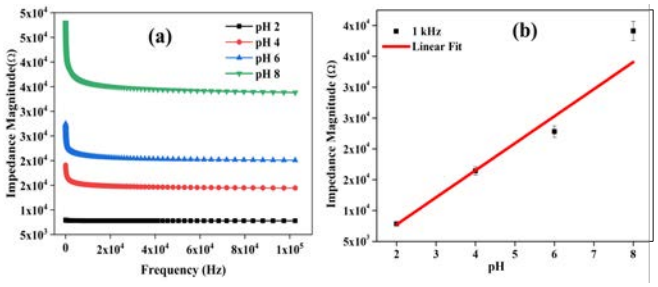

Fig. 8. (a) pH sensing performance of the sensor for soil samples and (b) Sensitivity of soil pH sensor for the selected frequency of 1 kHz.

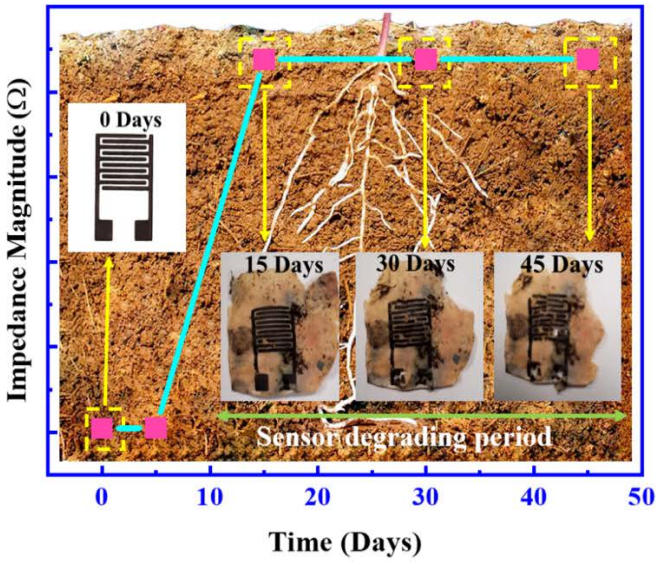

Fig. 9. The degradation process for pH sensor over 45 days.

corresponding pH level. The software module of the monitoring system is written in the Arduino integrated development environment (IDE) and the control code is developed using embedded C programming language. After the source code is generated and uploaded to the ESP8266, the device turns out to be smart to detect the pH levels with a fixed delay of around 15 sec.

ThingSpeak (IoT analytics platform) is used to monitor and visualize the live data streams in the IoT cloud platform. As depicted in Fig. 10a, the detected pH data is received and displayed in real time on a smart device. Fig. 10b is the front-end visualization system, which represents both previously recorded and real time pH measurements. While Fig. 10c represents the geographical information of the measurement spot of the pH sensor along with an easy display highlighting the pH levels. The supplementary Video S1 displays the real time pH sensing, where the pH level is measured at pH 2-8. Fig. 10 (d and e) shows the dynamic response and recovery time of the fabricated pH sensor, which is measured using a developed monitoring system. The response and recovery time for individual analytes (such as for pH 2 and 8) are different due to the variation in the interaction between the functional group with H^+ and OH^-. This also contributes to the delay in measurement for varying pH levels. As observed in the obtained results, pH 2 provides a quick response time (10 sec)

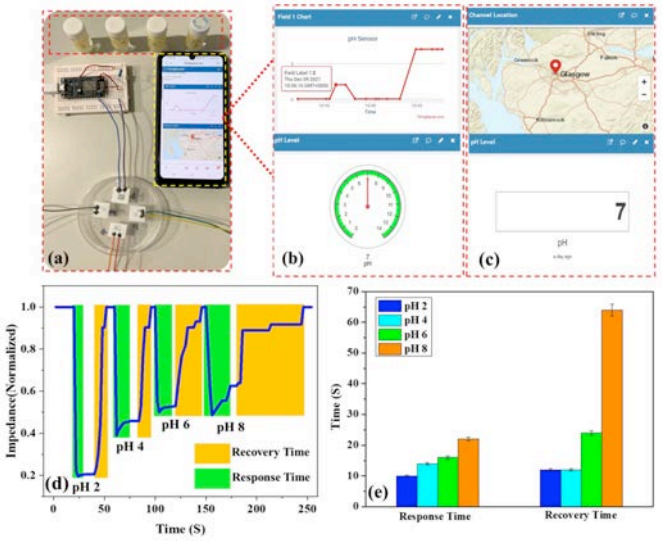

Fig. 10. (a) IoT enabled pH monitoring system, (b) Data displayed in the application showing the change in the values at multiple cycles (c) Data displaying the geographical location of the measurement spot and (d & e) Dynamic pH sensor response and recovery time (pH 2-8).

which is comparatively more rapid than of pH 8 (22 sec). Moreover, the recovery time for any sensor is the time needed for it to retain its initial state as soon as eliminates the analyte. The recovery time required for the sensor at pH 8 (64 sec) is almost 5 times slower compared to that of pH 2 (12 sec). This essentially depends on the analyte elimination process by the sensor and reaches at its initial state.

IV. Conclusion

In summary, the screen-printed flexible and disposable pH sensors on the paper substrate was developed using a modified using ZnO layer on screen printed IDE using G-C ink. Whilst the nanostructured active layer provides large surface areas and binding sites for the target H^+ and OH^- ions, the biocompatible and disposable paper-based sensor platforms allow ease of operation for soil pH monitoring. The fabricated sensor shows nearly three orders of change in impedance in the pH range of 2 – 9. The sensor exhibits a high sensitivity of 5.27 KΩ /pH (2-8) with a correlation coefficient (R^2) of 0.99 and displays high stability in the response. The wireless data transmission was also explored to show the usage of developed sensors for remote monitoring in applications such as digital agriculture. Beyond pH measurement, the sensor could also be used to monitor the humidity and temperature change caused in the soil surface and could be coupled as a multivariant detection sensor array.

References

[1] L. Santos *et al.*, "WO3 nanoparticle-based conformable pH sensor," *ACS Appl. Mater. Interfaces*, vol. 6, no. 15, pp. 12226–12234, 2014, doi: 10.1021/am501724h.

[2] D. Kurniawan, B. A. Anjali, O. Setiawan, K. K. Ostrikov, Y. G. Chung, and W.-H. Chiang, "Microplasma Band Structure Engineering in Graphene Quantum Dots for Sensitive and Wide-Range pH Sensing," *ACS Appl. Mater. Interfaces*, vol. 14, no. 1, pp. 1670–1683, 2022, doi: 10.1021/acsami.1c18440.

[3] M. V. Storey, B. van der Gaag, and B. P. Burns, "Advances in on-line drinking water quality monitoring and early warning systems," *Water Res.*, vol. 45, no. 2, pp. 741–747, 2011, doi: 10.1016/j.watres.2010.08.049.

[4] L. Laysandra, D. Kurniawan, C.-L. Wang, W.-H. Chiang, and Y.-C. Chiu, "Synergistic Effect in a Graphene Quantum Dot-Enabled Luminescent Skinlike Copolymer for Long-Term pH Detection," *ACS Appl. Mater. Interfaces*, 2021, doi: 10.1021/acsami.1c18077.

[5] N. Padmanathan, H. Shao, and K. M. Razeeb, "Multifunctional Nickel Phosphate Nano/Microflakes 3D Electrode for Electrochemical Energy Storage, Nonenzymatic Glucose, and Sweat pH Sensors," *ACS Appl. Mater. Interfaces*, vol. 10, no. 10, pp. 8599–8610, 2018, doi: 10.1021/acsami.7b17187.

[6] D. Ramotowski and W. Shi, "Nitrapyrin-based nitrification inhibitors shaped the soil microbial community via controls on soil pH and inorganic N composition," *Appl. Soil Ecol.*, vol. 170, no. October 2021, p. 104295, 2022, doi: 10.1016/j.apsoil.2021.104295.

[7] M. Chung *et al.*, "Fabrication of a Wearable Flexible Sweat pH Sensor Based on SERS-Active Au/TPU Electrospun Nanofibers," *ACS Appl. Mater. Interfaces*, vol. 13, no. 43, pp. 51504–51518, 2021, doi: 10.1021/acsami.1c15238.

[8] W. Vonau, W. Oelßner, U. Guth, and J. Henze, "An all-solid-state reference electrode," *Sensors Actuators, B Chem.*, vol. 144, no. 2, pp. 368–373, 2010, doi: 10.1016/j.snb.2008.12.001.

[9] M. Zea, A. Moya, M. Fritsch, E. Ramon, R. Villa, and G. Gabriel, "Enhanced Performance Stability of Iridium Oxide-Based pH Sensors Fabricated on Rough Inkjet-Printed Platinum," 2019, doi: 10.1021/acsami.9b03085.

[10] M. Jović *et al.*, "Large-scale layer-by-layer inkjet printing of flexible iridium-oxide based pH sensors," *J. Electroanal. Chem.*, vol. 819, no. August, pp. 384–390, 2018, doi: 10.1016/j.jelechem.2017.11.032.

[11] M. Zea, A. Moya, M. Fritsch, E. Ramon, R. Villa, and G. Gabriel, "Enhanced Performance Stability of Iridium Oxide-Based pH Sensors Fabricated on Rough Inkjet-Printed Platinum," *ACS Appl. Mater. Interfaces*, vol. 11, no. 16, pp. 15160–15169, 2019, doi: 10.1021/acsami.9b03085.

[12] S. K. Arya, S. Saha, J. E. Ramirez-Vick, V. Gupta, S. Bhansali, and S. P. Singh, "Recent advances in ZnO nanostructures and thin films for biosensor applications: Review," *Anal. Chim. Acta*, vol. 737, pp. 1–21, 2012, doi: 10.1016/j.aca.2012.05.048.

[13] M. Chakraborty, J. Kettle, and R. Dahiya, "Electronic Waste Reduction Through Devices and Printed Circuit Boards Designed for Circularity," *IEEE J. Flex. Electron.*, vol. 1, no. 1, pp. 4–23, 2022, doi: 10.1109/jflex.2022.3159258.

[14] Z. Wang *et al.*, "Correlation between Photocorrosion of ZnO and Lattice Relaxation Induced by Its Surface Vacancies," *J. Phys. Chem. C*, vol. 125, no. 5, pp. 3242–3255, 2021, doi: 10.1021/acs.jpcc.0c11260.

[15] G. K. Mani, M. Morohoshi, Y. Yasoda, S. Yokoyama, H. Kimura, and K. Tsuchiya, "ZnO-Based Microfluidic pH Sensor: A Versatile Approach for Quick Recognition of Circulating Tumor Cells in Blood," *ACS Appl. Mater. Interfaces*, vol. 9, no. 6, pp. 5193–5203, 2017, doi: 10.1021/acsami.6b16261.

[16] A. K. A, N. K. S K, A. A. Aniley, F. R. E, and S. Bhansali, "Hydrothermal Growth of Zinc Oxide (ZnO) Nanorods (NRs) on Screen Printed IDEs for pH Measurement Application," *J. ofThe Electrochem. Soc.*, vol. 166, no. 9, pp. B3264–B3270, 2019, doi: 10.1149/2.0431909je.

[17] E. S. Hosseini, S. Dervin, P. Ganguly, and R. Dahiya, "Biodegradable Materials for Sustainable Health Monitoring Devices," *ACS Appl. Bio Mater.*, vol. 4, no. 1, pp. 163–194, 2021, doi: 10.1021/acsabm.0c01139.

[18] N. Yogeswaran, E. S. Hosseini, and R. Dahiya, "Graphene Based Low Voltage Field Effect Transistor Coupled with Biodegradable Piezoelectric Material Based Dynamic Pressure Sensor," *ACS Appl. Mater. Interfaces*, vol. 12, no. 48, pp. 54035–54040, 2020, doi: 10.1021/acsami.0c13637.

[19] E. S. Hosseini, L. Manjakkal, D. Shakthivel, and R. Dahiya, "Glycine-Chitosan-Based Flexible Biodegradable Piezoelectric Pressure Sensor," *ACS Appl. Mater. Interfaces*, vol. 12, no. 8, pp. 9008–9016, 2020, doi: 10.1021/acsami.9b21052.

[20] M. A. Kafi, A. Paul, A. Vilouras, E. S. Hosseini, and R. S. Dahiya, "Chitosan-Graphene Oxide-Based Ultra-Thin and Flexible Sensor for Diabetic Wound Monitoring," *IEEE Sens. J.*, vol. 20, no. 13, pp. 6794–6801, 2020, doi: 10.1109/JSEN.2019.2928807.

[21] S. Deshpande, S. Bhand, and G. Bacher, "Investigation of the effect of metallization ratio and side shift on the interdigitated electrodes performance for biochemical sensing," *J. Appl. Electrochem.*, vol. 51, no. 6, pp. 893–904, 2021, doi: 10.1007/s10800-021-01549-x.

[22] L. Freire, M. J. Carmezim, M. G. S. Ferreira, and M. F. Montemor, "The passive behaviour of AISI 316 in alkaline media and the effect of pH: A

combined electrochemical and analytical study," *Electrochim. Acta*, vol. 55, no. 21, pp. 6174–6181, 2010, doi: 10.1016/j.electacta.2009.10.026.
[23] M. T. Ghoneim *et al.*, "Recent Progress in Electrochemical pH-Sensing Materials and Configurations for Biomedical Applications," *Chem. Rev.*, vol. 119, no. 8, pp. 5248–5297, 2019, doi: 10.1021/acs.chemrev.8b00655.
[24] L. Manjakkal, D. Szwagierczak, and R. Dahiya, "Progress in Materials Science Metal oxides based electrochemical pH sensors : Current progress and future perspectives," *Prog. Mater. Sci.*, vol. 109, no. December 2019, p. 100635, 2020, doi: 10.1016/j.pmatsci.2019.100635.
[25] K. Arshak, E. Gill, A. Arshak, and O. Korostynska, "Investigation of tin oxides as sensing layers in conductimetric interdigitated pH sensors," *Sensors Actuators, B Chem.*, vol. 127, no. 1, pp. 42–53, 2007, doi: 10.1016/j.snb.2007.07.014.
[26] S. Al-Hilli and M. Willander, "The pH response and sensing mechanism of n-type ZnO/electrolyte interfaces," *Sensors*, vol. 9, no. 9, pp. 7445–7480, 2009, doi: 10.3390/s90907445.
[27] J. Hong *et al.*, "AC frequency characteristics of coplanar impedance sensors as design parameters," *Lab Chip*, vol. 5, no. 3, pp. 270–279, 2005, doi: 10.1039/b410325d.
[28] A. K. Aliyana *et al.*, "Machine learning-assisted ammonium detection using zinc oxide/multi-walled carbon nanotube composite based impedance sensors," *Sci. Rep.*, vol. 11, no. 1, pp. 1–10, 2021, doi: 10.1038/s41598-021-03674-1.

Akshaya Kumar Aliyana received his Master's in Electronics with the first rank from Mangalore University, India in 2016. He is a recipient of INSPIRE Fellowship from the Department of Science and Technology (DST), Govt. of India. He was a Newton Bhabha visiting researcher with Electronics and Nanoscale Engineering Research Division, BEST Group, University of Glasgow, U.K. He is currently working towards his Ph.D. at the Department of Electronics, Mangalore University, India. His research focus is on the area of Biosensors, Embedded systems, and the Internet of Things. He has presented 29 International/National conference papers, has co-authored 17 Journal publications and 04 book chapters.

Priyanka Ganguly is a lecturer of Analytical Chemistry at the London metropolitan University. She received her Ph.D. in Nanotechnology from the Institute of Technology Sligo, Ireland in 2020. She worked as a Marie Curie Early-Stage researcher in the Bendable Electronics and Sensing Technologies (BEST) group at the University of Glasgow. Her research interests include the synthesis and characterization of nanomaterials for various energy and environmental applications such as electrochemical sensors, physical sensors, supercapacitor devices, ink formulation for printed electrodes and photocatalytic applications. She has authored/co-authored more than 25 research articles and presented in several international and national conferences. She also received the Institute of Chemistry of Ireland Postgraduate Award in 2020 and the Kathleen Longsdale Chemistry RIA prize of 2022.

Ajay Beniwal received his B.Tech. and M.Tech. degree in Electronics and Communication Engineering from Kurukshetra University Kurukshetra, India, in 2013 and 2015, respectively, and a Ph.D. degree from the Department of Electronics and Communication Engineering, Indian Institute of Information Technology, Allahabad, Prayagraj, India in 2021. He is currently a Marie Curie Early-Stage Researcher with the Bendable Electronics and Sensing Technologies (BEST) Group, Electronics and Nanoscale Engineering, University of Glasgow, U.K. His current research interest includes material characterization and thin film technology, electronic sensor devices, printed and flexible electronics, for healthcare and agriculture applications.

Naveen Kumar S K is a Professor of the Department of Electronics at Mangalore University, India. He received his Ph.D. in Electronics (2001) from the University of Mysore, India. Prof. Kumar is a multidisciplinary researcher with a focus on smart electrochemical biosensors and printed electronics for applications in agriculture, healthcare, and pollution control. Previously, he served as an Assistant Professor at the Department of Electronics, University of Mysore (2002-2013). Prof. Kumar has co-authored over 78 Journal publications and 94 International/National conference papers.

Ravinder Dahiya (Fellow, IEEE) is Professor of Electronics and Nanoengineering in the University of Glasgow, U.K. He is the leader of Bendable Electronics and Sensing Technologies (BEST) research group. His group conducts fundamental and applied research in flexible and printable electronics, tactile sensing, electronic skin, robotics, and wearable systems. He has authored or co-authored more than 450 publications, books and submitted/granted patents and disclosures. He has led several international projects. He is President (2022-23) of the IEEE Sensors Council. He is the Founding Editor in Chief of IEEE JOURNAL ON FLEXIBLE ELECTRONICS (J-FLEX) and has served on the editorial boards of Scientific Report, IEEE SENSORS JOURNAL (2012-2020) and IEEE TRANSACTIONS ON ROBOTICS (2012-2017). He was the Technical Program co-chair of IEEE Sensors 2017 and IEEE Sensors 2018 and has been General Chair of several conferences including IEEE FLEPS (2019, 2020, 2021), which he founded in 2019. He holds the prestigious EPSRC Fellowship and received in past the Marie Curie and Japanese Monbusho Fellowships. He has received several awards, including 2016 Microelectronic Engineering Young Investigator Award (Elsevier), 2016 Technical Achievement Award from the IEEE Sensors Council and 12 best paper awards as author/coauthor in International Conferences and Journal.